Catal Lett (2013) 143:1188–1194
DOI 10.1007/s10562-013-1054-y

Palladium Supported on Functionalized Mesoporous Silica as an Efficient Catalyst for Suzuki–Miyaura Coupling Reaction

Guoheng Zhang · Peiyu Wang · Xiufang Wei

Received: 23 April 2013 / Accepted: 23 June 2013 / Published online: 2 July 2013

Abstract Mesoporous SBA-15 was modified with organic functional groups by co-condensation method. The functionalized mesoporous silica can be loaded with palladium and the resulting material used as a catalyst for the Suzuki–Miyaura coupling reactions. Highly dispersed and uniform palladium nanoparticles could be detected using transmission electron microscopy. The Pd-SBA-15 nanocomposite with controlled molar ratio of amino groups to palladium exhibits an excellent catalytic activity and low Pd leaching for the Suzuki–Miyaura coupling reaction. The catalyst can also be reused at least six recycles in air with only a minor loss of activity.

Keywords Mesoporous silica · Suzuki–Miyaura coupling reactions · Catalytic activity

1 Introduction

Palladium-catalyzed cross coupling reactions, such as the Suzuki–Miyaura reaction, have become the standard methodologies for the synthetic organic chemists to construct biaryl units [1–3]. Although homogeneous Pd catalysts have gained enormous relevance, industrial applications of these reactions remain challenging, because the homogeneous catalysts require the use of ligands, which are often not easy to handle. In addition, the removal of the catalysts from reaction mixtures and products is difficult in most cases, which is a drawback especially when these reactions are applied in the pharmaceutical field.

Palladium supported on the hosts may offer solutions for some of the above mentioned problems such as mesoporous silicas [4], carbon nanotubes (CNT) [5–7], metal–organic frameworks (MOF) [8], montmorillonites [9], and zeolites [10]. Among these hosts, mesoporous silicas, especially SBA-15, have been widely investigated thanks to their controllable size, composition and morphology, which are highly desirable for catalytic applications [11].

Although there have been several approaches for loading palladium nanoparticles (Pd NPs) onto mesoporous silica using solution infiltration and surface grafting methods, development of a general and facile method to obtain Pd NPs supported on mesoporous silica remains challenging due to its easy agglomeration and leach without protecting groups [12–16]. It is fairly accepted that amino groups can bind strongly to noble metal nanoparticles [17, 18]. Palladium supported on the amino group functionalized zeolite [19], fumed silica [20], and mesoporous MCM-41 [21] are efficient catalysts. Moreover, the diamine functionalized mesoporous materials are attracting much attention due to the strong absorbing and chelating performance of ethylenediamine groups [22]. More recently, controlled Au and Cu nanoparticles were supported in ordered mesoporous materials functionalized by diamine groups on the pore surface [17, 18, 23]. However, so far the Suzuki–Miyaura reactions catalyzed by palladium anchored on diamine functionalized SBA-15 catalyst have not been studied.

In our present work, a novel approach to prepare Pd supported on SBA-15 with high Pd loading and high Pd dispersion was developed. Mesoporous SBA-15 was modified with organic functional groups by co-condensation

G. Zhang (✉) · P. Wang
Key Laboratory for Electronic Materials of the State National Affairs Commission of PRC, Northwest University for Nationality, Lanzhou 730030, Gansu, China
e-mail: dzclsys@163.com

X. Wei
College of Bailie Engineering and Technology, Lanzhou City University, Lanzhou 730070, China

method. Then, Pd^{2+} ions were grafted and fixed compactly onto the organo-functionalized SBA-15 via the coordination bonds. The resulting sample thus was reduced by formalin to obtain Pd supported on SBA-15 (Pd-SBA-15). The catalytic activity of the Pd-SBA-15 was investigated by Suzuki–Miyaura reactions.

2 Experimental Procedure

Triblock poly (ethylene oxide)-*b*-poly (propylene oxide)-*b*-poly (ethylene oxide) copolymer ($EO_{20}PO_{70}EO_{20}$, MW = 5,800, Pluronic P123) was from Aldrich. Hydrochloric acid (HCl), tetraethoxysilane (TEOS), [3-(2-aminoethyl aminopropyl)] trimethoxysilane (ATMS), 4-*tert*-butyltoluene, phenylboronic acid, aryl bromide, potassium carbonate, toluene and palladium chloride were all purchased from Shanghai Reagent Factory Two Company. All the chemicals used in the present investigation were in the as-received forms without any further purification. The deionized water was used in all experiments.

2.1 Synthesis

NH-SBA-15 prepared by co-condensation Method. In this method, 1 g of (3-aminopropyl)trimethoxysilane (APTMS) (6 mmol) was added 1 h after the addition of TEOS following the regular synthesis of SBA-15 [24]. The molar ratio of APTMS to TEOS was 0.3. After being stirred at room temperature for 1 day, the mixture was transferred into an autoclave and heated at 100 °C for 24 h. The product was collected by filtration and dried overnight at 100 °C. Then, the solvent extraction was performed by stirring 0.5 g of the product in the mixture of 50 mL of ethanol and 50 mL of diethyl ether for 24 h [25]. The extraction products are denoted as NH-SBA-15. SBA-15 mesoporous silica powder was also prepared for comparison.

In a typical experiment, the NH-SBA-15 (0.5 g) was added to a solution of $PdCl_2$ (0.05 g) in water (5 mL) and stirred for 24 h at room temperature. The mixture was filtrated and washed 3 times with 5 mL water under ultrasonic for 1 min, and then dried in vacuum. Afterward, the dried sample was stirred with 5 mL of 1 M hydrazine hydrate at 60 °C for 3 min. The mixture was then filtrated, washed three times with 10 mL water, and dried at room temperature. Finally, a dark gray powder (Pd-SBA-15) was obtained. For comparison of the catalytic activity in Suzuki–Miyaura reaction, the other two samples (C1 and C3) were also prepared in the similar way, but 0.1 g $PdCl_2$ was replaced by 0.05 g $PdCl_2$ for C1 and 0.2 g $PdCl_2$ for C2. Also, the other one sample (C3) was prepared in the similar way, but NH-SBA-15 was replaced by SBA-15 for C3.

2.2 Catalytic Testing

A typical experimental procedure was as follows: A mixture of aryl bromide (10.0 mmol), phenylboronic acid (13.0 mmol), potassium carbonate (18.0 mmol), the catalyst (0.05 mol % with respect to palladium), and 4-*tert*-butyltoluene (500 mg) as an internal standard for gas chromatograph (GC) analysis were stirred in water (3 mL) at 80 °C under N_2 atmosphere. Every 15 min, an aliquot of reaction mixture ($\sim$100 μL) was sucked out with degassed syringe, filtered and washed with brine and diethyl ether. After completion, the reaction mixture was diluted with water (20 mL) and extracted with ether (3 × 20 mL). The combined extract was washed with brine (2 × 20 mL) and dried over Na_2SO_4. After evaporation of the solvent under reduced pressure, the residue was chromatographed (silica gel, ethyl acetate-hexane: 1:9) to obtain the desired products. The products were confirmed by comparing the H and ^{13}C NMR and mass spectral data with authentic samples. The Pd concentration was measured with inductively coupled plasma atomic emission spectrometry (ICP-AES). For the measurement of the Pd leaching from the Pd-SBA-15 catalyst in the course of reaction, the solution was filtrated and the organic compounds were evaporated. The residue obtained by calcination at 600 °C in air for 2 h was dissolved in aqua regia. The recycling test was performed with bromobenzene and phenylboronic acid under the same reaction condition as described above. Each time, the catalyst was isolated from the reaction mixture at the end of the reaction, washed with water and diethyl ether, and then dried at 100 °C under vacuum. The dried catalyst was then reused in the next run.

2.3 Instrumentation

Pd elemental analysis of the nanocomposites was performed on a Thermo IRTS advantage ICP-AES. N elemental analyses of the nanocomposites were performed on a VarioEL CHNS elemental analyzer. Fourier transform infrared spectrometry (FTIR) was carried on a Nicolet Nexus 670 Spectrometer. The X-ray powder diffraction (XRD) experiments were carried out on a Rigaku D/Max-2400 X-ray diffractometer using Cu K_α radiation. CO chemisorption measurements were taken at 298 K using a homemade pulse flow system. Prior to measurements, samples were subjected to a pretreatment involving exposure to hydrogen flow for 1 h at 300 °C, then the sample was cooled down to room temperature in pure N_2 stream. The transmission electron microscopy (TEM) observations of the Pd-SBA-15 nanocomposite were carried out on a JEM 1010 operating at an acceleration voltage of 100 kV. Nitrogen adsorption–desorption isotherms were measured by a NOVA 2000e surface area and pore size analyzer. The

specific surface areas were evaluated using Brunauer-Emmett-Teller (BET) method. Pore size distribution was calculated using the Barrett-Joyner-Halenda (BJH) method based on the desorption branch of the isotherms, and the pore size was reported from the peak position of the distribution curve. The pore volume was taken from a single-point adsorbed volume at a relative pressure P/P_0 of 0.97.

3 Results and Discussion

3.1 Structure and Morphology of Nanocomposites

FT-IR spectra of SBA-15 and NH-SBA-15 were shown in Fig. 1. Bands at similar 458, 813 and 1,080 cm^{-1} in both spectra of SBA-15 and NH-SBA-15 have been assigned to characteristic vibrations of Si–O–Si bridges crosslinking the silica network. The band at 1,630 cm^{-1} in the spectrum of SBA-15 is attributed to the adsorbed water; and a broad band at 3,432 cm^{-1} in the spectrum of SBA-15 can be assigned to the hydrogen-bonding silanol groups and adsorbed water. The weak band at 3,740 cm^{-1} in the spectrum of SBA-15 is attributed to the fundamental stretching vibrations of silanol groups on the surface, which is invisible after the condensation of silanol groups with organic silane. A weak peak at around 696 cm^{-1} in the spectrum of NH-SBA-15 is attributed to N–H bending vibration. In the spectrum of NH-SBA-15 the absorbance peak of the C–N stretching vibration in the wave number range of 1,000–1,200 cm^{-1} cannot generally be resolved due to its overlap with the absorbance of Si–O–Si stretch in the range 1,000–1,130 cm^{-1} and that of Si–CH_2–R stretch in the range 1,200–1,250 cm^{-1}. The bands at 1,480 and 1,578 cm^{-1} in the spectrum of NH-SBA-15 are attributed to the NH and NH_2 bending vibrations, respectively. The presence of the band at 2,936 cm^{-1} in the spectrum of NH-SBA-15 is associated with CH_2 vibrations corresponding to the CH stretching. These further confirm the incorporation of organic species in the framework.

Figure 2 shows the small angle XRD patterns of SBA-15, NH-SBA-15, and Pd-SBA-15. The samples all exhibit three well-resolved peaks, one intense peak at about 0.85–0.90° and two weak peaks at about 1.50–1.55° and 1.70–1.75° which can be indexed as (100), (110), and (200) reflections of two-dimensional hexagonal symmetry (*P6mm*) [21] (the two-dimensional hexagonal structure of Pd-SBA-15 will be verified by the TEM analysis). SBA-15 shows a diffraction peak at 0.87° which corresponds to the (100) *d*-spacing of 10.2 nm (shown in Table 1). The repeat distance a_0 between two neighboring pore centers of the hexagonal structure is 11.8 nm (by the equation $a_0 = 2d_{100}/\sqrt{3}$ [27]). In comparison to the diffraction pattern of SBA-15, no significant change is observed in the diffraction pattern of NH-SBA-15 and Pd-SBA-15, indicating the retention of the hexagonal pore array structure. The (100) *d*-spacing of NH-SBA-15 and Pd-SBA-15 are 10.1 and 10.0 nm; the corresponding repeat distance a_0 between two neighboring pore centers are 11.7 and 11.5 nm (listed in Table 1).

Figure 3 displays the wide angle XRD patterns of Pd-SBA-15. The peaks at $2\theta = 40.1°$, 46.7°, 68.1°, and 82.0° are the (111), (200), (220), and (311) diffractions of the fcc Pd, respectively. The average grain size of the Pd nanoparticles in the Pd-SBA-15 nanocomposite was estimated from the full width at half maximum of the diffraction peaks using Scherrer equation. The average grain size of the Pd nanoparticles in the Pd-SBA-15 nanocomposite is 3.4 nm. The Pd content in the Pd-SBA-15 nanocomposite was measured with ICP-AES and the N content was measured with CHNS elemental analyzer. The palladium

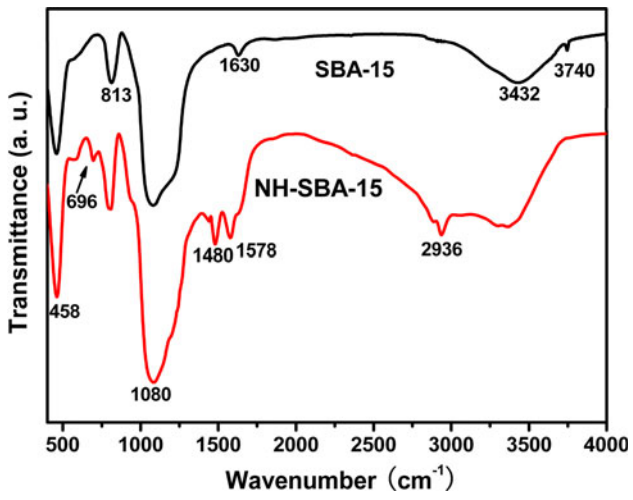

Fig. 1 FT-IR spectrum of *SBA-15* and *NH-SBA-15*

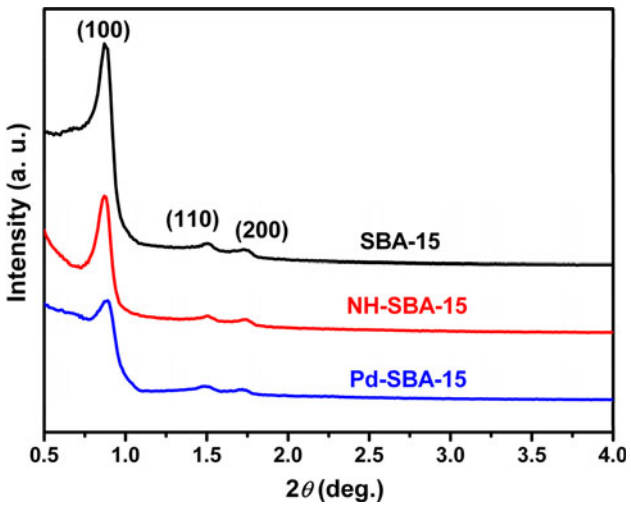

Fig. 2 Small angle XRD patterns of *SBA-15*, *NH-SBA-15*, and *Pd-SBA-15*

Table 1 Physiochemical properties of SBA-15, NH-SBA-15, and Pd-SBA-15 nanocomposites obtained from small angle XRD and N_2 adsorption–desorption

Sample	d_{100} (nm)	a_0 (nm)[a]	BET surface area ($m^2\ g^{-1}$)	BJH pore size (nm)	Pore volume ($cm^3\ g^{-1}$)
SBA-15	10.2	11.8	846	8.3	1.02
NH-SBA-15	10.1	11.7	420	7.9	0.71
Pd-SBA-15	10.0	11.5	373	7.6	0.60

[a] $a_0 = 2d_{100}/\sqrt{3}$

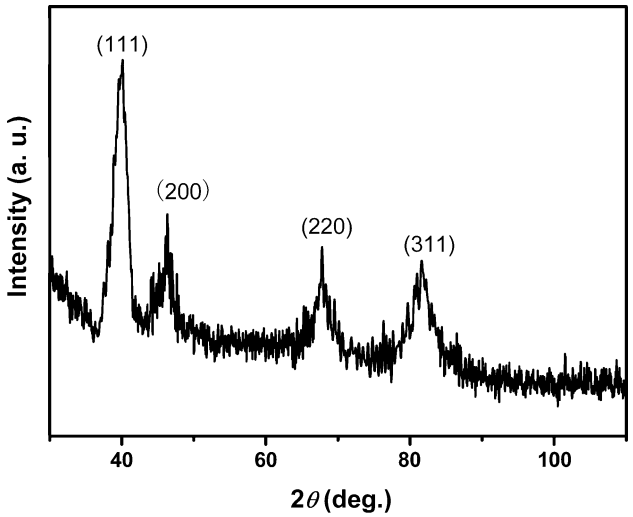

Fig. 3 Wide angle XRD pattern of Pd-SBA-15

and nitrogen contents of Pd-SBA-15 nanocomposite were found to be 0.43 and 0.83 mmol g^{-1}, respectively.

The metal dispersion and metal surface of the catalyst were studied by the CO chemisorption. A stoichiometry of CO/Pd = 1/1 [28–30] and a Pd surface density of 1.27×10^{19} atoms m^{-2} were used for calculations [31]. The Pd dispersion of Pd-SBA-15 is determined to be 33 %. In comparison, the Pd/SBA-15 materials prepared using PH-adjusting method on SBA-15 showed Pd dispersions between 24 and 27 % [25]. The metal dispersion of the Pd-SBA-15 is higher than this of Pd/SBA-15. This indicates that Pd-SBA-15 prepared by our novel preparation process exhibits a higher metal dispersion.

The TEM observations provide the direct observation of the morphology and the distribution of the Pd nanoparticles in Pd-SBA-15. The TEM micrograph in Fig. 4a clearly shows that Pd-SBA-15 has a hexagonal pore array structure. The dark spots of the Fig. 4b are the Pd nanoparticles. It can be clearly seen in Fig. 4 that highly dispersed Pd nanoparticles with the size between 3–6 nm encapsulated in the ordered pores of the mesoporous silica without any agglomeration.

The nitrogen adsorption/desorption isotherms and the pore size distribution for SBA-15, NH-SBA-15, and Pd-SBA-15 are shown in Fig. 5. The isotherm for SBA-15 (circle in Fig. 5) presents the type IV with a H1-type hysteresis loop defined by IUPAC [32]. This type of hysteresis loop is associated with capillary condensation and desorption in open-ended cylindrical mesopores [26, 32]. Generally, the shape of the isotherm is preserved after a modification step. Hysteresis loops with the similar shapes reveal the absence of pore clogging [26]. The pore structure parameters of the samples are summarized in Table 1. A specific surface area of 846 $m^2\ g^{-1}$, a pore volume of

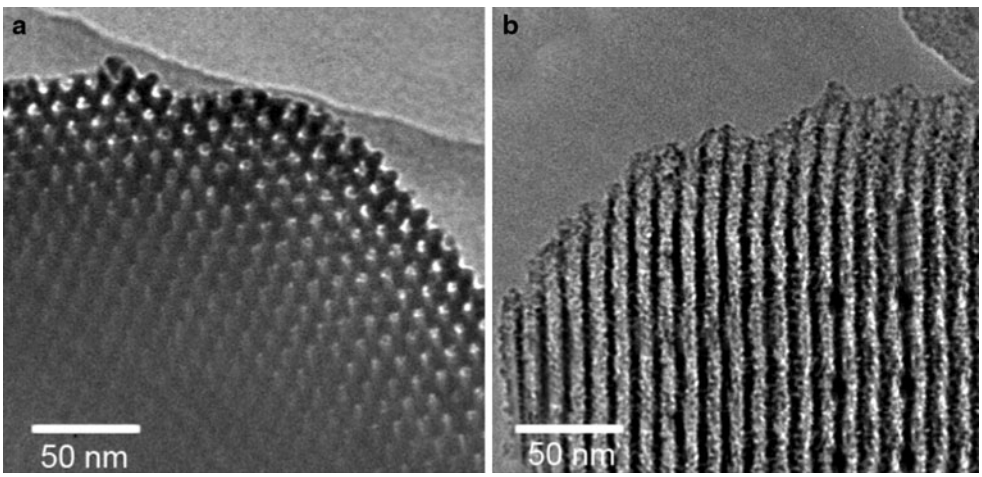

Fig. 4 TEM micrograph of Pd-SBA-15: top view (**a**); side view (**b**)

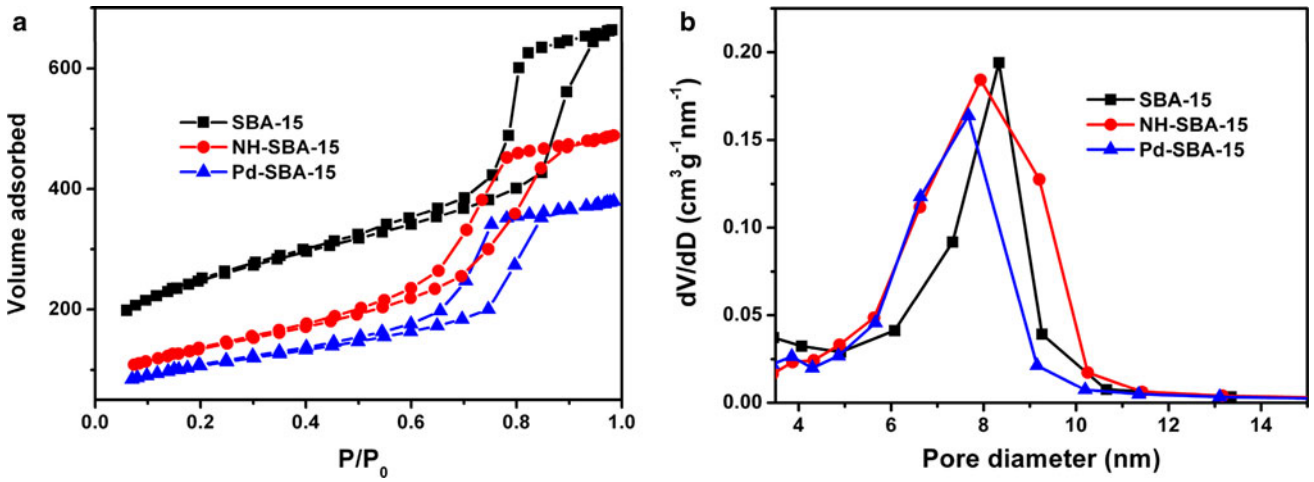

Fig. 5 Nitrogen adsorption–desorption isotherms (**a**) and pore size distributions (**b**) of *SBA-15*, *NH-SBA-15*, and *Pd-SBA-15*

1.02 cm^3 g^{-1}, and a pore size of 8.3 nm are obtained from the isotherm of SBA-15. The BET surface areas of the NH-SBA-15 and Pd-SBA-15 are 420 and 373 m^2 g^{-1}, respectively. The pore volumes for NH-SBA-15 and Pd-SBA-15 are 0.68 and 0.60 cm^3 g^{-1}, respectively. The pore sizes for NH-SBA-15 and Pd-SBA-15 are 7.9 and 7.6 nm, respectively. Compared to the BET surface area, pore volume, and BJH pore size of SBA-15, the decreased BET surface area, pore volume, and BJH pore size for NH-SBA-15 can be due to the occupation of large organic groups in the pore channels. With the incorporation of Pd nanoparticles in the channels of NH-SBA-15, the BET surface area, pore volume and BJH pore size of the Pd-SBA-15 nanocomposite decrease slightly further.

3.2 Catalytic Characteristics of Pd-SBA-15

The catalytic performance of each prepared silica-immobilized amino-palladium complex was probed in the Suzuki–Miyaura coupling reaction between aryl bromides and phenylboronic acid to give the corresponding biphenyl products. The activity of catalyst and Pd leaching in the reaction are strongly affected by the molar ratio of functional groups to Pd of the nanocomposite [12]. Table 2 shows the catalytic activity and Pd leaching as a function of the N:Pd molar ratio for the reaction of bromobenzene and phenylboronic acid as the model reaction. The catalyst activity of C3 was the lowest and the Pd leaching was the highest among all the samples, these shown that the existence of amino groups could prevent the agglomeration of Pd nanoparticles in the synthesis reaction and also could prevent the leaching of Pd nanoparticles in the catalytic reactions. As the N:Pd molar ratio increases, the Pd leaching of the reaction decreases. An N:Pd molar ratio of 4:1 for the C1 sample, the Pd leaching is least but the activity of the catalyst is lowest in these three samples (Table 2, entry 1). At the standard N:Pd molar ratio of 2:1 for Pd-SBA-15, the Pd concentration in solution at the end of the reaction is as little as 0.10 ppm (Table 2, entry 2). At an N:Pd molar ratio of 1:1 for the C2 sample, the catalyst shows an increased leaching (compared with entry 1 and 2). An N:Pd molar ratio of 2:1 is the optimal N:Pd molar ratio since it exhibits the highest activity and a moderate Pd leaching.

To investigate the reaction scope with Pd-SBA-15 as the catalyst, various aryl bromides with different substituents were employed. Fast conversion of aryl bromides were achieved in all cases as indicated by gas chromatography (GC) analysis. The results are summarized in Table 3. The Suzuki reaction of bromobenzene with phenylboronic acid

Table 2 Catalytic activity and leaching as a function of N to Pd molar ratio with the bromobenzene and acrylic acid as the model reaction

Entry	Sample	N content (mmol g^{-1})	Pd content (mmol g^{-1})	N:Pd	Yield[a]	Pd leaching (ppm)
1	C1	0.85	0.21	4:1	60	0.05
2	Pd-SBA-15	0.84	0.41	2:1	98	0.10
3	C2	0.82	0.80	1:1	89	0.40
4	C3	/	0.38	/	72	0.50

The reaction was carried out at 80 °C, 1 h with 0.05 mol% Pd-SBA-15 as catalyst

[a] Determined by GC analysis using 4-*tert*-butyltoluene as an internal standard

Table 3 Suzuki–Miyaura coupling reactions of aryl halides over Pd-SBA-15

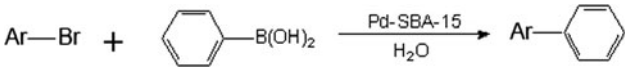

Entry[a]	Ar	Yield[b]
1	Ph	98
2	4-$CH_3OC_6H_4$	96
3	4-$CHOC_6H_4$	97
4	4-$CH_3C_6H_4$	98
5	4-$CH_3OCOC_6H_4$	99
6	4-$O_2NC_6H_4$	96
7	4-CNC_6H_4	98
8	2-Pyridyl	90
9	2-Thienyl	92
10[c]	Ph	98
11[d]	4-$CHOC_6H_4$	95
12[e]	Ph	21
13[e]	Ph	78

[a] Reaction conditions: aryl bromides (10.0 mmol), phenylboronic acid (13.0 mmol), K_2CO_3 (18.0 mmol), catalyst (0.05 mol % Pd), water (3 mL), 80 °C, 1 h

[b] Determined by GC analysis using 4-*tert*-butyltoluene as an internal standard

[c] The reaction was catalyzed by 0.08 mol % Pd-SBA-15 related to the amount of aryl halides at 80 °C for 1 h [13]

[d] The reaction was catalyzed by 1 mol % NH-Pd-SH-SBA(SS) related to the amount of aryl halides at 80 °C for 12 h with DMF/H_2O (20/1) as solution [33]

[e] The reaction was catalyzed by Pd_{10} (entry 12) or Pd_5Au_5 (entry 13) nanoparticles supported on SBA-15 at 100 °C for 0.5 h with microwave-assisted [34]. Pd was 0.5 mol % related to the amount of aryl halides [34]

also furnished an excellent yield of biphenyl in 1 h (Table 3, entry 1). We also examined the reaction with several substituted aryl bromides and phenylboronic acid under the optimized reaction conditions. The reactions were all carried out at 80 °C in 1 h, affording biphenyl products with high yields (Table 3, entry 2–7). The coupling reactions of heteroaryl bromides such as 2-bromothiophene and 2-bromopyridine with phenylboronic acid also gave the corresponding coupled products in 92 and 90 % yields, respectively (Table 3, entry 8 and 9). These results show that the catalyst has high activity in the Suzuki–Miyaura reactions. Compared to the Pd nanoparticles in carbon thin film-lined SBA-15 nanoreactors [13], the Pd-SBA-15 shows relatively higher catalytic activity in the Suzuki–Miyaura reactions (Table 3, entry 1 and 10). We also compared the activity of our catalyst with these of NH-Pd-SH-SBA (Table 3, entry 1 and 11) and Pd_{10} (Table 3, entry 1 and 12) or Pd_5Au_5 (Table 3, entry 1 and 13) nanoparticles supported on SBA-15, the Pd-SBA-15 also shows relatively higher catalytic activity in the Suzuki–Miyaura reactions [33, 34]. We attributed this to the high dispersion of the Pd nanoparticles throughout the mesoporous silica structure and high surface area of catalysts.

Table 4 Recycling test for Suzuki–Miyaura coupling reaction

Recycle	1	2	3	4	5	6	7
Yield	98	98	96	97	92	90	80

0.05 mol % Pd-SBA-15 was used in this reaction

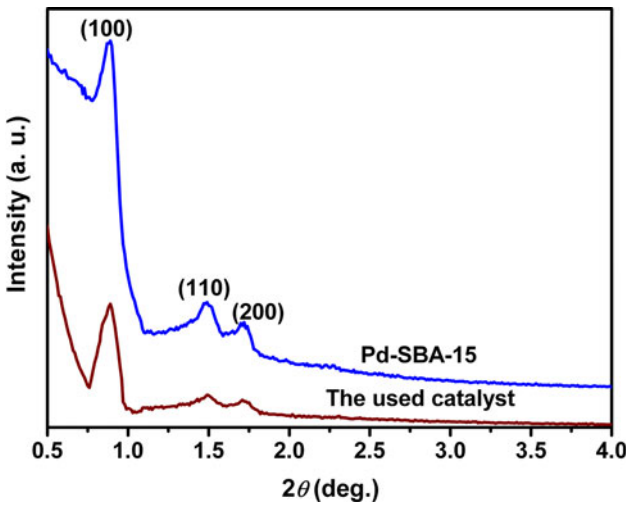

Fig. 6 Small angle XRD patterns of *Pd-SBA-15* and *the used Pd-SBA-15 catalyst* recovered from the sixth recycle

As shown in Table 4, this Suzuki–Miyaura coupling reaction of bromobenzene and phenylboronic acid exhibits high yield at least up to 90 % until sixth recycling usage, but the conversion drops to 80 % in the seventh recycling usage. Therefore, the catalyst Pd-SBA-15 can be reused and keeps its high catalytic activity in catalyst recycling for Suzuki–Miyaura coupling reaction. Detailed studies were carried out on Pd-SBA-15 that was recovered from the sixth recycle in the reaction between bromobenzene and phenylboronic acid. The palladium and the nitrogen contents in the used catalyst recovered from the sixth recycle are determined to be 4.1 and 0.79 mmol g^{-1} by the elemental analysis, respectively. Compared to the fresh catalyst, both the Pd and N content were slightly decreased, indicating they both leached in the solution during reactions. CO chemisorption of the used catalyst shows that there is a little decrease in Pd dispersion (Pd dispersion 28 % compared to 33 % of fresh catalyst). These indicate that there are a little Pd aggregation after six recycles. The small angle XRD pattern of the used catalyst recovered from the sixth recycle (Fig. 6) shows that the structure of catalyst is maintained even when the catalyst is used for six recycles. Based on the investigations above, a minor decrease of the catalytic activity in recycle reaction can be

attributed to minor Pd leaching, N leaching and a little Pd agglomeration in the course of reaction.

4 Conclusions

Pd supported on SBA-15 (or Pd-SBA-15) with high Pd loading and high Pd dispersion was prepared by functionalizing SBA-15 with ATMS using co-condensation method, grafting palladium ions on the functionalized SBA-15, and reducing palladium ions in the functionalized SBA-15 with hydrazine hydrate. The Pd-SBA-15 nanocomposite has a Pd loading of the 0.43 mmol g^{-1}. Highly dispersed uniform Pd nanoparticles are distributed in the hexagonal channels of SBA-15. The surface area, the pore volume, and the pore size decrease slightly with the incorporation of the Pd nanoparticles in the pore channels of SBA-15. The catalyst provides excellent catalytic activity for bromobenzene and phenylboronic acid reactions. Although there is a little Pd, N leaching and and a little Pd agglomeration accompanied with the decreasing of Pd dispersion during reaction, the catalyst can be reused six times with only a minor decrease of activity.

Acknowledgments This work was supported by the Fundamental Research Funds for the Central Universities, China. (Grant No. zyz2012057), Natural Science Foundation of Gan Su Province (Grant No. 0803RJZA008), China.

References

1. Martin R, Buchwald SL (2008) Acc Chem Res 41:1461
2. Littke AF, Fu GC (2002) Angew Chem Int Ed 41:4176
3. Yin LX, Liebscher J (2007) Chem Rev 107:133
4. Zhang R, Ding W, Tu B, Zhao D (2007) Chem Mater 19:4379
5. Pan X, Fan Z, Chen W, Ding Y, Luo H, Bao X (2007) Nat Mater 6:507
6. Castillejos E, Debouttiere P-J, Roiban L, Solhy A, Martinez V, Kihn Y, Ersen O, Philippot K, Chaudret B, Serp P (2009) Angew Chem Int Ed 48:2529
7. Serp P, Castillejos E (2010) ChemCatChem 2:41
8. Wu CD, Hu A, Zhang L, Lin WB (2005) J Am Chem Soc 127:8940
9. Mitsudome T, Nose K, Mori K, Mizugaki T, Ebitani K, Jitsukawa K, Kaneda K (2007) Angew Chem Int Ed 46:3288
10. Mandal S, Roy D, Chaudhari RV, Sastry M (2004) Chem Mater 16:3714
11. Vos DED, Dams M, Sels BF, Jacobs PA (2002) Chem Rev 102:3615
12. Webb JD, MacQuarrie S, McEleney K, Crudden CM (2007) J Catal 252:97
13. Zhi J, Song D, Li Z, Lei X, Hu A (2011) Chem Commun 47:10707
14. Hea C, Zhanga F, Yueb L, Shanga X, Chena J, Hao Z (2012) Appl Catal B 111–112:46
15. Huang J, Yin J, Chai W, Liang C, Shen J, Zhang F (2012) New J Chem 36:1378
16. Morèrea J, Tenorioa MJ, Torralvob MJ, Pandoa C, Renuncioa JAR, Cabãnasa A, Super J (2011) Fluids 56:213
17. Gu J-L, Shi J-L, You G-J, Xiong L-M, Qian S-X, Hua Z-L, Chen H-R (2005) Adv Mater 17:557
18. Hao X-Y, Zhang Y-Q, Wang J-W, Zhou W, Zhang C, Liu S (2006) Microporous and Mesoporous Materials 88:38
19. Crooks RM, Zhao M, Sun L, Chechik V, Yeung LK (2001) Acc Chem Res 34:181
20. Zhao SF, Zhou RX, Zheng XM (2004) J Mol Catal A: Chem 211:139
21. Zhou J, Zhou R, Mo L, Zhao S, Zheng X (2002) J Mol Catal A: Chem 178:289
22. Wang X, Chan JCC, Tseng Y-H, Cheng S (2006) Micro Meso Mater 95:57
23. Zhu H, Lee B, Dai S, Overbury SH (2003) Langmuir 19:3974
24. Levasseur B, Ebrahim AM, Bandosz TJ (2012) Langmuir 28:5703
25. Li C, Zhang Q, Wang Y, Wan H (2008) Catal Lett 120:126
26. Zhao D, Sun J, Li Q, Stucky GD (2000) Chem Mater 12:275
27. Zhao D, Feng J, Huo Q, Melosh N, Frederickson GH, Chmelka BF, Stucky GD (1998) Science 279:548
28. Mahata N, Vishwanathan V (2000) J Catal 196:262
29. Ali SH, Goodwin JG (1998) J Catal 176:3
30. Panpranot J, Pattamakomsan K, Goodwin JG, Praserthdam P (2004) Catal Commun 5:583
31. Anderson JR (1975) Structure of metallic catalysts. Academic, London
32. Sing KSW, Everett DH, Haul RAW, Moscou L, Pierotti RA, Rouquerol J, Siemieniewska T (1985) Pure Appl Chem 57:603
33. Nohair B, MacQuarrie S, Crudden CM, Kaliaguine S (2008) J Phys Chem C 112:6065
34. Zheng Z, Li H, Liu T, Cao R (2010) J Catal 270:268